ACS OMEGA

http://pubs.acs.org/journal/acsodf

Article

Combining Multiple Methods for Recycling of Kish Graphite from Steelmaking Slags and Oil Sorption Performance of Kish-Based Expanded Graphite

Jihui Li, Ruochen Liu, Liqiang Ma, Lubin Wei, Lili Cao, Wanci Shen, Feiyu Kang, and Zheng-Hong Huang*

Cite This: *ACS Omega* 2021, 6, 9868−9875

Read Online

ACCESS | Metrics & More | Article Recommendations

ABSTRACT: The utilization of industrial waste as renewable resources is an essential issue of sustainable development. Kish graphite is a precipitate of excess carbon generated during the cooling of molten iron and one of the byproducts associated with steel slags. The scale-up recycling of kish graphite from steelmaking slags is a promising way to develop natural graphite alternatives. However, only one means cannot work efficiently because of the unusual occurrence of associated impurities; combining multiple separation methods is the solution. In this paper, we proposed an integrated beneficiation process, pneumatic separation−flotation−sonication−magnetic separation, to recycle kish graphite flakes with a high graphitization degree and investigated the sorption performance of various oils on kish-based expanded graphite. The new process avoided shortages such as the sediments of iron particles in the flotation cell and the loss of clean graphite in the magnetic separation. Consequently, the carbon content of kish graphite reached ∼95% after separation and >99% after acid leaching. The macroscopic structural defects of kish particles created more active sites, made the intercalation of KG-GICs faster, and yielded better-staged compounds. The kish graphite-based expanded graphite presented an octopus-like shape and exhibited an expansion volume of ∼150 mL/g. Furthermore, the developed macropore structure of the obtained kish graphite-based expanded graphite led to a superior sorption performance for oils. This work supplies one feasible and promising way to recycle kish graphite from steelmaking slags and use it.

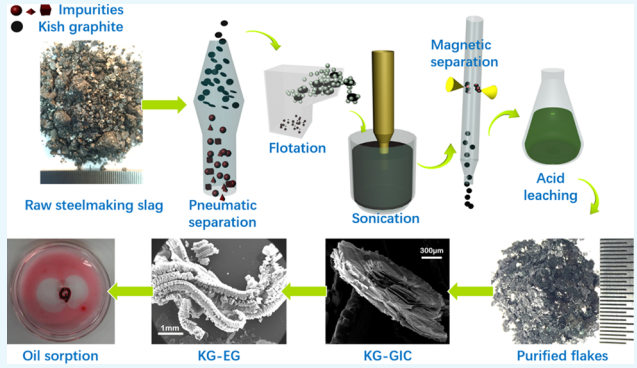

INTRODUCTION

Graphite is a nonrenewable, nonpolar, and nonmetallic mineral and plays essential roles in many technological and industrial applications. Nature graphite (NG) has some important properties, such as chemical inertness, thermal stability, high electrical conductivity, and lubricity. These properties make it suitable for many applications, including electronics, lubricants, metallurgy, and steelmaking.[1] Some emerging technologies in large-scale fuel cells, batteries, and lightweight high-strength composites substantially increase the world demand for graphite.[2−5] Therefore, graphite is of far greater strategic importance globally than before.

Kish graphite (KG), a precipitate of excess carbon generated during the cooling of molten iron, is one of the byproducts associated with steel slags.[6,7] So far, the steel output of China has steadily ranked the first place in the world, accompanying with discharge of large amounts of slags. The stockpiling of steel slags has caused serious environmental pollution and land wastage. Due to KG's high crystallinity, the properties similar to those of NG,[8−12] and the significantly low price, making the recovery of KG technically feasible has a tremendous environmental and economic significance.[13]

Some beneficiation methods have been tried to recycle KG from steel slags.[14−18] Among them, froth flotation, which is the most common approach used for NG separation, gets the most attention. It is based on the distinct hydrophobicity difference of surfaces between the nonpolar graphite and polar impurity. However, in our experiments, we found that the settling of iron impurities in cells hindered the flotation process. Laverty[14] investigated the effects of magnetic separation on KG from steelmaking waste. However, their barely satisfactory results indicated that many KG flakes behaved as a magnetic material

Received: February 1, 2021
Accepted: March 17, 2021
Published: April 2, 2021

https://doi.org/10.1021/acsomega.1c00591
ACS Omega 2021, 6, 9868−9875

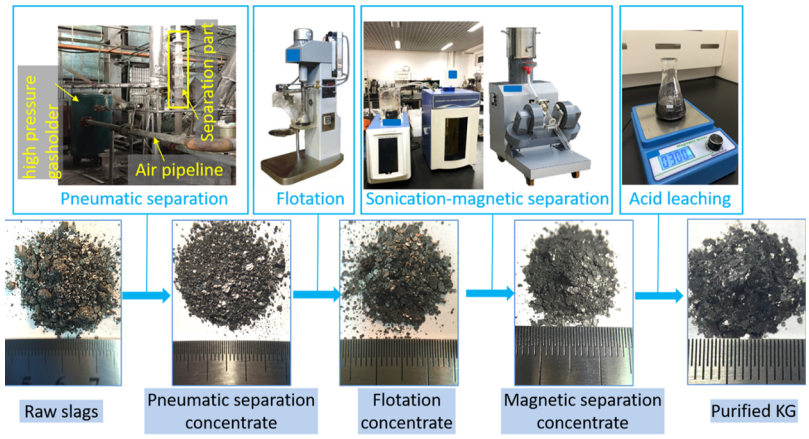

Figure 1. Schematic illustration of the PFSM beneficiation process and acid leaching of KG.

because they were embedded into small iron spheres or entrained by the high ratio of magnetic particles. Some others' reports also indicated that one single process could not work well as the particular occurrence of associated impurities for KG recycling. Therefore, the process development of technologies combined for KG recycling has become a promising solution.

Due to the immaturity of the recovery technologies and the particularity of KG's structure, its application has not been launched on a large scale. KG-based graphene,[16] sensors,[19] graphite foils,[20] cathode material for batteries,[2,21,22] and some other material application studies are just on the lab scale. Thus, it is not wise to explore an application in the field of traditional graphite or other layer structure materials.[23] It is better to develop a large utilization application field that matches Kish graphite properties under the premise of massive recovery technology.

In the present study, we proposed the pneumatic separation−flotation−sonication−magnetic separation (PFSM) process. First, the pneumatic separation was used to remove the dissociated, coarse, and heavy impurities, flotation was employed to eliminate the fine impurities selectively, and then magnetic separation combined with sonication liberation was used to remove the remaining entrained iron. The PFSM process avoided the shortages such as the sediments of iron particles in the flotation cell and the loss of clean graphite in magnetic separation. The structure characterization shows that KG has excellent crystallinity, and kish-based expanded graphite (KG-EG) held more mesopores than nature graphite-based expanded graphite (NG-EG). The sorption test demonstrates that KG-EG had good equilibrium adsorption capacities and adsorption rates for various oils. This work makes the recovery of KG with high recovery and grade from steel slags feasible. The excellent adsorption performance of kish-based expanded graphite shows one valuable application prospect of KG.

EXPERIMENTAL SECTION

Materials and Reagents. Steel slags were collected from Nanjing Iron and Steel Group Co., Ltd, Nanjing, Jiangsu Province, China. The natural graphite (lateral size >80 mesh, carbon content >99.9%) was obtained from Ulanqab Darsen Graphite New Materials Co., Ltd. In the flotation process, kerosene (0#, Sinopec) was used as a collector, and 2-octanol (assay 97%, Sigma-Aldrich) was used as a frother. Hydrochloric acid (assay 37%, Sigma-Aldrich) was used in the leaching process. Concentrated sulfur acid (assay ≥98%, Aldrich) was used as intercalates to prepare GICs.

Beneficiation by the PFSM Process and Purification of KG. Aside from KG flakes, the impurities, such as iron, iron oxide, quartz, calcium carbonate, and magnesium carbonate, are present in raw slag samples. The beneficiation of KG by the PFSM process followed by the acid leaching flowsheet is shown schematically in Figure 1. A variable-diameter pulsed airflow separator (the structure and implementation of the airflow separator are given in the patent[24]) was used to remove the coarse and heavy impurities in the first stage. Scavenging and cleaning froth flotation processes using 180 g/L solid content feed, 20 g/kg collector, and 2 g/kg frother were conducted to remove the smaller impurities. An ultrasonic bath (YDC-1200E, frequency = 40 kHz, power = 840 W) was employed to dissociate the embedded iron particles from KG flakes. A magnetic separation tube featuring a magnetic field of 2500 GS was used to eliminate the magnetic iron. Following physical beneficiation, hydrochloric acid leaching was utilized to remove iron, iron oxide, calcium hydroxide, magnesium hydroxide, and other remaining impurities strongly associated with or embedded into KG flakes. The KG concentrate (10 g) was added to HCl (10%, 200 mL), stirred at 50 °C for one h, and filtrated. This leaching process was repeated until the filtrate was colorless. Finally, the purified KG was obtained after washing with deionized water and drying in an oven at 60 °C for 1 h.

Preparation of Graphite Intercalation Compounds. The purified kish graphite (1 g) was put into a porous polyethylene capsule and immersed in concentrated sulfuric acid. The galvanostatic method was used to carry out intercalation reaction for a specific time (at 0.9 A for 0−4 h) by a DC power supply.[25] Graphite intercalation compounds (GICs) were prepared by filtering, washing, and drying the reactants. Finally, expanded graphite (EG) particles were obtained after heating the GICs at 950 °C for 6 s in a muffle furnace.

Characterization. The morphologies and energy-dispersive X-ray spectroscopy (EDS) of EG samples were examined by scanning electron microscopy (SEM, MERLIN Compact). The lattices of host graphite and GICs were characterized by X-ray diffraction (XRD, Rigaku D/max 2500 V, target = Cu, step width = 0.01°, acceleration voltage = 40 kV). The graphitization degree was determined by XRD featuring an

https://doi.org/10.1021/acsomega.1c00591
ACS Omega 2021, 6, 9868−9875

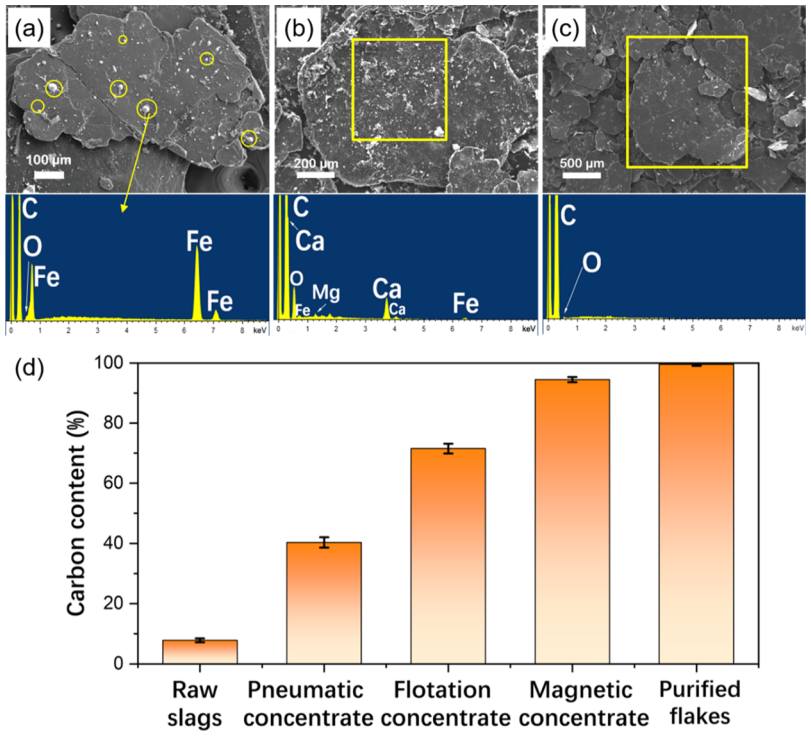

Figure 2. Micrographs and the corresponding selected area EDS of the flotation concentration (a), magnetic concentration (b), purified flakes (c) of kish graphite, and carbon contents of KG samples at different stages (d).

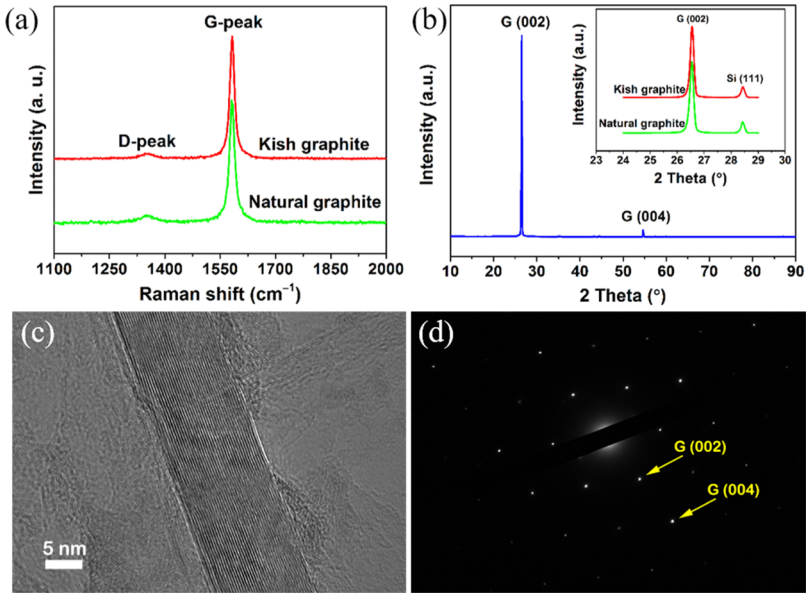

Figure 3. Raman spectra (a) and XRD patterns (b) of purified KG and NG, and the inset illustrates XRD patterns using the Si inner standard, HR-TEM image (c) and SAED pattern of acid-leached KG (d).

internal Si standard. The stages of GICs were tested using the originally resulted samples with the intercalate but not the residual GICs washed by water (it should be cautious to prevent samples from spilling or contacting the instrument). Raman scattering spectra were obtained using a 532 nm laser (HORIBA Scientific, LabRAM HR Evolution). High-resolution transmission electron microscopy (HR-TEM) images were obtained using a JEOL JEM-2100 F instrument. A mercury porosimeter was used to investigate EG's pore-size distributions featuring different bulk densities.

RESULTS AND DISCUSSION

Beneficiation and Purification of KG. The pneumatic separation gave an excellent performance for removing coarse and heavy impurity particles from steel slags. The carbon content had an evident rise from ~10% for the raw material to ~40% after pneumatic beneficiation (Figure 2d). This is due to the drag difference caused by the density, size, and shape of the impurity particles and kish flakes.[26−28] However, to make the carbon content meet the requirements of application or

https://doi.org/10.1021/acsomega.1c00591
ACS Omega 2021, 6, 9868−9875

materialization, some follow-up deeper beneficiation processes are in demand.

The carbon content of KG after flotation was ~75% (Figure 2d). The morphology combined with EDS (Figure 2a) illustrates that, after flotation, KG flakes still contained some small, embedded iron particles (marked by yellow circles) with ~10 μm in diameter, which is consistent with the research result of Liu.[13]

Laverty[14] proposed how the magnetic separation was used at the first stage as a rough concentration treatment to remove iron impurities from pristine steelmaking slag. When trying to duplicate Laverty's method, we found that his process sequence caused the KG flakes embedded by iron spheres to be attracted as the magnetic product. Meanwhile, some KG flakes not embedded by iron are lost into the magnetic products either by the entrainment of magnetic matter. Therefore, the position of the magnetic separation in the flowsheet is critical. Unlike the previous study, in our process, the sonication was applied after flotation to liberate impurities from KG flakes and improved the following magnetic separation efficiency. Data indicate that our design decreased the yield of magnetic products to 4.57% from 83.87% of Laverty's method and considerably reduced KG loss. Because most iron particles in flotation concentration were discarded in this process, the carbon content of KG after magnetic beneficiation reached up to ~95% (Figure 2b,d).

After acid leaching, the carbon content of purified KG reached >99% (Figure 2d). The EDS data indicate that the leached KG concentrates were mostly composed of elemental C and small amounts of O. Other impurity elements, such as Fe, Mg, and Ca, were not detected (Figure 2c).

In summary, the significant increase of samples' carbon content at different beneficiation stages demonstrates that the PFSM process was efficient in recovering KG with high grade.

Graphitization Degree of KG. KG owns high crystallization and graphitization degree.[12] The Raman spectra (Figure 3a) and XRD patterns (Figure 3b) of KG and NG are similar. However, their graphitization degrees calculated from XRD patterns (101.5% for KG and 98.6% for NG) using Si inner standard indicate that the crystallinity of KG was superior to that of NG. The higher graphitization degree was also tested by Walker and An.[12,18] Walker attributed the smaller interlayer spacing and higher graphitization degree of KG to the high pressure when molten iron contracted during cooling. The regular lattice fringe pattern of purified KG was studied using HR-TEM (Figure 3c). The associated selected area electron diffraction (SAED, Figure 3d) pattern shows an ideal hexagonal phase crystal structure, which coincides well with the results of XRD and Raman spectra.

Macroscopic Structure Defects of EG. Some irregular structures of KG flakes are observed (Figure 4a,b): the edges of KG, consisted of many "peninsulas and bays", were zigzag and different from those of the NG flakes featuring suborbicular or nearly elliptical morphology (Figure 4c); the surface of KG flakes had many holes and raised platforms (marked by circles and arrows), while NG was flat. It was suggested that the small holes were formed by the vacations from etched impurity particles embedded in KG flakes or by the decreased lateral size of adjacent bonding KG particles caused by the condition deteriorating during their growth in molten iron.

The raised platform, which was amplified due to the slight expansion along the C axis (Figure 4d), was supposed to be a small kish particle that adhered to the surface of a big KG flake

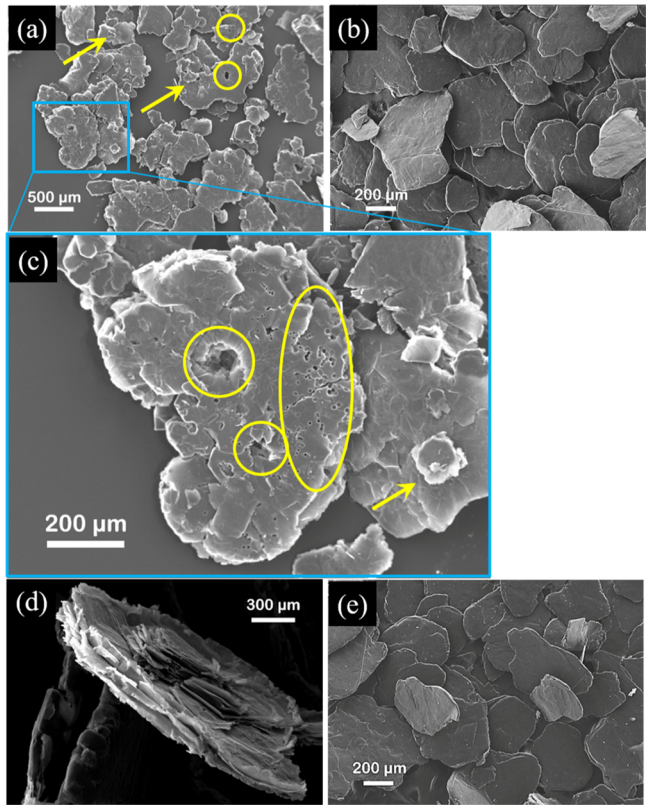

Figure 4. SEM images of KG flakes (a), NG flakes (b), and magnification of the selected square on one piece of KG (c), a piece of KG-GICs (d), and a chip of NG-GICs (e).

and intergrew since its nucleation. However, these holes and raised platforms are different from the pores and hillocks observed by Bourelle[29] using a scanning tunneling microscope, which are microstructural defects. Moreover, Bourelle attributed their formation to the diffusion of iron impurities during the growth of KG. Compared with the almost defect-free morphology of the NG flakes and NG-GICs (Figure 4e), the edges of the KG-GIC particles exhibited obvious predelamination. The large number of macroscopic structure defects and a more extended perimeter of KG created more contact sites for intercalation reaction, and the excessive intercalation resulted in predelamination.

Preparation of KG-EG. The KG-EG exhibited an expansion volume of ~150 mL/g, and some KG-EG particles presented octopus-like morphology featuring branches and were different from the worm-like NG-EG particles (Figure 5a,b). As illustrated in the SEM images (Figure 5c,d), every branch separated from the trunk was one entire vermicular particle and presented a well-developed porous structure. The octopus-like structure, combined with several vermicular particles, indicated that adjacent KG nucleations spontaneously combined to form one integrated graphite flake and synchronously grow, while KG was generated during the molten iron cooling.[7] When rapidly heating the graphite intercalation compound particles, the adhesion was broken to some extent with expansion and the octopus-like structures formed.

At a specific expansion temperature, the pore structure and expansion volume of EG are mainly governed by the quality of GICs, which is expressed in terms of stages.[30−32] The "stage" in intercalation nomenclature essentially refers to the number

https://doi.org/10.1021/acsomega.1c00591
ACS Omega 2021, 6, 9868−9875

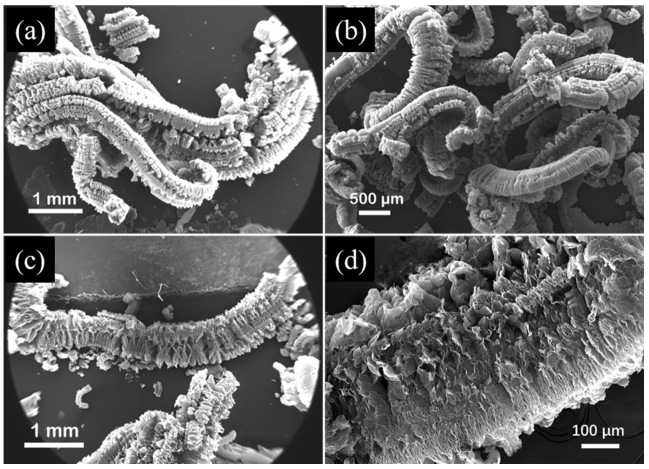

Figure 5. SEM images of one octopus-like KG-EG particle (a), NG-EG particles (b), one of the KG-EG branches (e), and the cross section of one KG-EG branch along the *C* axis (d).

of carbon sheets that lie between alternate intercalant layers. Hence, stage one is the GIC system with the highest level of intercalant concentration.[33] The stepwise formation of GICs of increasingly higher concentration can be detected by the stepwise left shift of characteristic peaks of GICs via XRD. The characteristic peak positions represent the space of the graphite layers. Figure 6a shows the XRD spectra of NG-GICs and KG-GICs under electrochemical intercalation for different times. According to the results, in the initial 5 min, the characteristic peaks obviously left shifted with the prolonging of intercalation time, representing the increase of the space of carbon atom layers. Concretely, from 0 to 3 min, the *G* (002) peak (at 26.38°) of graphite disappeared, and the *G* (002)′ peak (at 25.60°) of GICs in stage 5 gradually emerged. From 3 to 4 min, the *G* (002)′ peak rapidly decreased until it disappeared, at the same time, the characteristic peak [*G* (002)″ peak, at 24.92°] of GICs in stage 4 appeared and increased.

Comparing the intercalation time that KG-GICs and NG-GICs reached the same stage, the results suggest that the host KG cost little time and was easier to create high order GICs. For 2 min, the NG-GICs were just stage 5; however, the KG-GICs had been stage 5 + stage 4 (the majority). The time to reach stage 2 was 15 min for NG-GICs, but 4 min for KG-GICs. Dresselhaus[34] found the small, thin samples intercalate more quickly and often yield a better-staged, more homogeneous material than large and thick samples. These macroscopic structural defects, such as the holes, raised platforms, branches, and crevices of concomitant kish particles, create more reactive sites and divide the flake into several small pieces, improving the intercalation processing of KG-GICs.

After the characteristic peak of stage 2 remained for a long time, a typical system containing stages 1 and 2 is shown in Figure 6a, and it well follows the Daumas-Herold model.[35] The XRD also suggests that GICs were mixtures, not the compounds of one stage, but generally mixture with several stages. Under the electrochemical intercalation condition, KG-GIGs always cost a shorter time to transfer to higher stages (Figure 6b). This indicates that KG-GICs hold better intercalation kinetic than NG-GICs. The mixture model and the time consumption of reaching different stages via electricity agree with the galvanostatic method well.[33]

KG-EG possesses a suitable pore structure for the sorption of macromolecular organics. Figure 7a,b illustrates that, for both KG-EG and NG-EG, the volumes of micropores and mesopores were significantly smaller than those of macropores. However, KG-EG exhibited a more significant number of macropores from 50 to 200 μm. A similar pore structure was observed by Xing[23] in his study to use expanded vermiculite as a template to synthesize carbon nanosheets for high-performance lithium-ion batteries. The macropores larger than 10 μm play a vital role in the sorption of macromolecular organics such as oils and dyes.[36,37] The SSA of KG-EG was about twice as large as that of NG-EG (Figure 7c), and the total pore area of KG-EG was higher than that of NG-EG, too.

Sorption Performance of Oils on KG-EG. As shown in Figure 8, for the sorption of various oils on KG-EG and NG-EG, overall, the sorption capacities increased as the sorbates' viscosities increased. KG-EG's equilibrium sorption capacities were always higher, and the equilibrium sorption times were shorter than those of NG-EG, although the latter exhibited a higher expansion volume than the former.

Both the pores in the EG particles and the twine-room play essential parts in the oil sorption. For oil sorption, low-viscosity oils are absorbed within the pores inside wormlike particles, while high-viscosity oils are absorbed into the pores and the intertwined space among particles.[38] Zheng, Zhao, and Cao[38−40] measured the volumes of NG-EG particles and twine-room formed by intertwined wormlike particles using paraffin impregnation and pointed out that the relative percentage of twine-room volume to the total pore volume fluctuates in the narrow 73−77% range is regardless of expansion volume. This study found that the pristine fluffy EG particles bulk-collapsed and significantly shrunk after oil soak. During the liquid sorption, the EG particles' porous structure was deformed and shattered by the interfacial tension between EG and liquid.

Moreover, the decrease of the bulk was different for different oils, so it can be estimated that the twine-room sorption was not an inherent attribute of EG but was also affected by the adsorbent properties. KG-EG exhibited a smaller expansion volume but a larger pore volume than NG-EG, translating into a smaller twine room. Therefore, the higher sorption performance and faster sorption kinetics for the same oil indicated more inner sorption volume in KG-GE.

■ CONCLUSIONS

Based on the studies of multiple methods coupling for recycling kish graphite from steelmaking slags and the sorption performance of oils on KG-EG, the following conclusions can be drawn.

1. The PFSM (pneumatic separation−flotation−sonication−magnetic separation) process made the recycling of KG with high carbon content feasible. Pneumatic separation removed the heaviest and coarsest liberated impurities, flotation removed the fine impurities, and magnetic separation combined with sonication liberation furtherly eliminated the small and embedded iron impurities.
2. The macroscopic structural defects, such as the holes, raised platforms, branches, and crevices of concomitant kish particles, created more active sites, made the intercalation of KG-GICs faster, and yielded better-staged compounds.
3. KG-EG had good equilibrium adsorption capacities and adsorption rates for various oils and can be used as a

https://doi.org/10.1021/acsomega.1c00591
ACS Omega 2021, 6, 9868−9875

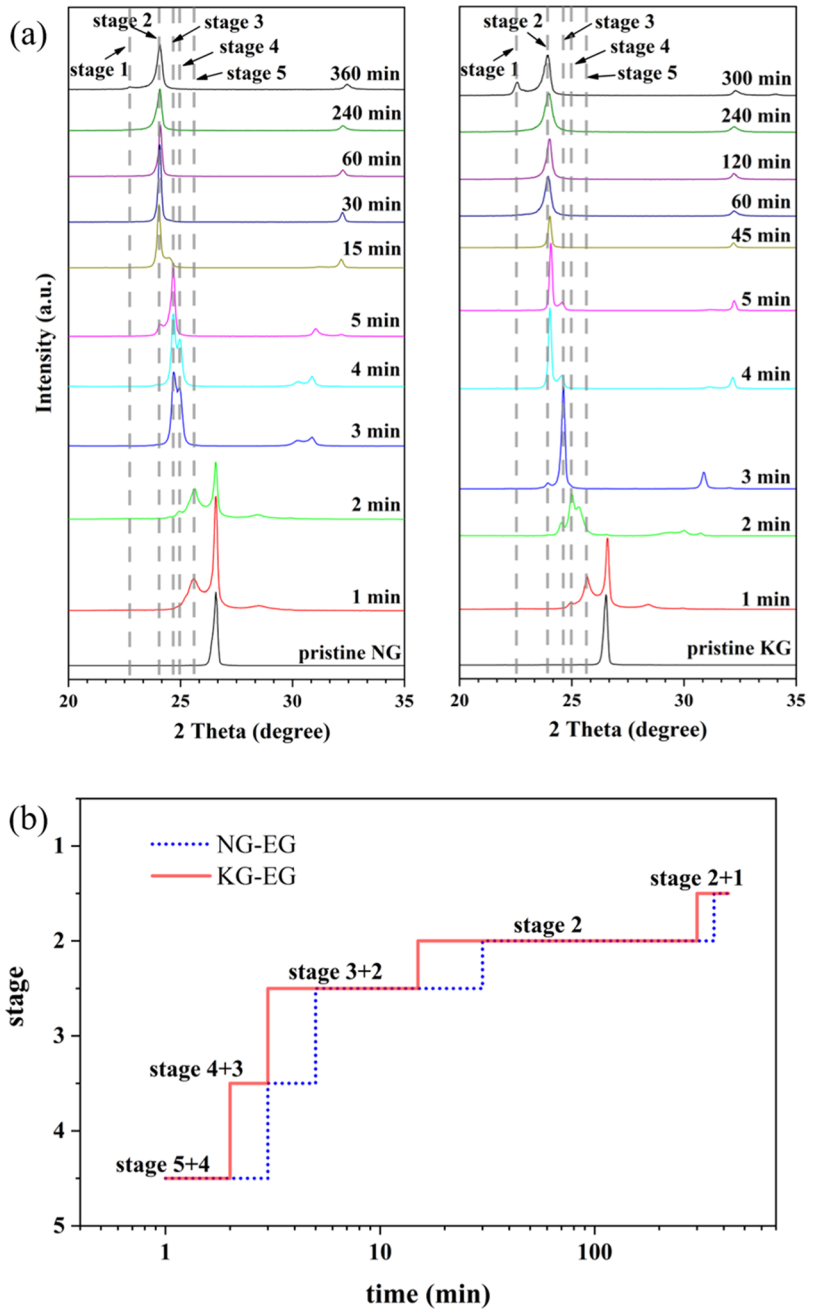

Figure 6. XRD patterns of NG- and KG-GICs obtained at different times by the electrochemical process (a) and the relation between GICs' stages and intercalation time (b).

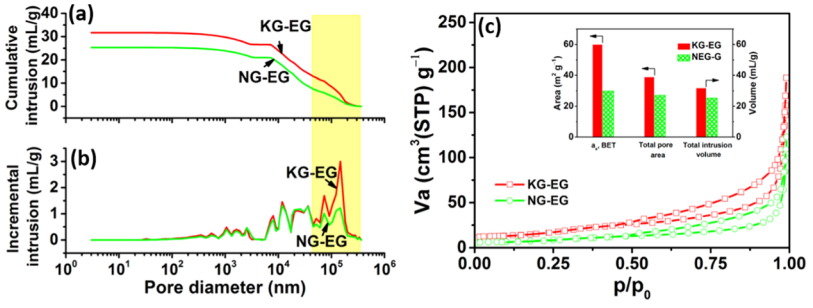

Figure 7. Pore-size distributions determined using a mercury porosimeter (a,b) and nitrogen adsorption−desorption isotherms (c) of KG-EG and NG-EG. The inset illustrates the SSA, total pore area, and total intrusion volume.

https://doi.org/10.1021/acsomega.1c00591
ACS Omega 2021, 6, 9868−9875

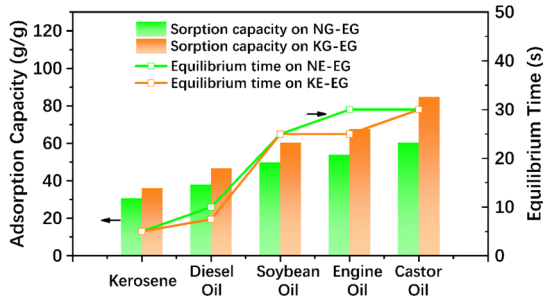

Figure 8. Sorption capacities and equilibrium times of KG-EG and NG-EG for oils.

low-cost alternative to the NG-GE material in oily wastewater treatment.

AUTHOR INFORMATION

Corresponding Author

Zheng-Hong Huang − *Key Laboratory of Advanced Materials (MOE), School of Materials Science and Engineering, Tsinghua University, Beijing 100084, China;* orcid.org/0000-0002-0591-6830; Email: zhhuang@mail.tsinghua.edu.cn

Authors

Jihui Li − *School of Chemical and Environmental Engineering, China University of Mining and Technology (Beijing), Beijing 100083, China; State Key Laboratory of Mineral Processing, Beijing 102628, China;* orcid.org/0000-0002-4748-0692

Ruochen Liu − *School of Chemical and Environmental Engineering, China University of Mining and Technology (Beijing), Beijing 100083, China*

Liqiang Ma − *School of Chemical and Environmental Engineering, China University of Mining and Technology (Beijing), Beijing 100083, China*

Lubin Wei − *School of Chemical and Environmental Engineering, China University of Mining and Technology (Beijing), Beijing 100083, China*

Lili Cao − *School of Chemical and Environmental Engineering, China University of Mining and Technology (Beijing), Beijing 100083, China*

Wanci Shen − *Key Laboratory of Advanced Materials (MOE), School of Materials Science and Engineering, Tsinghua University, Beijing 100084, China*

Feiyu Kang − *Key Laboratory of Advanced Materials (MOE), School of Materials Science and Engineering, Tsinghua University, Beijing 100084, China*

Complete contact information is available at: https://pubs.acs.org/10.1021/acsomega.1c00591

Notes

The authors declare no competing financial interest.

ACKNOWLEDGMENTS

This research was supported by the National Natural Science Foundation of China under Grant no. 52004294, the Open Foundation of State Key Laboratory of Mineral Processing under Grant no. BGRIMM-KJSKL-2019-19, and the Fundamental Research Funds for the Central Universities under Grant no. 2020YQHH09.

REFERENCES

(1) Rao, J.; Zhang, P.; He, S.; Li, Z.; Ma, H.; Shen, Z.; Miao, S. A review on the utilization of natural graphite and graphite-based materials. *SSci. Sin. Technol.* **2017**, *47*, 13−31.

(2) Xing, B.; Zhang, C.; Cao, Y.; Huang, G.; Liu, Q.; Zhang, C.; Chen, Z.; Yi, G.; Chen, L.; Yu, J. Preparation of synthetic graphite from bituminous coal as anode materials for high performance lithium-ion batteries. *Fuel Process. Technol.* **2018**, *172*, 162−171.

(3) Jara, A. D.; Betemariam, A.; Woldetinsae, G.; Kim, J. Y. Purification, application and current market trend of natural graphite: A review. *Int. J. Min. Sci. Technol.* **2019**, *29*, 671−689.

(4) Asenbauer, J.; Eisenmann, T.; Kuenzel, M.; Kazzazi, A.; Chen, Z.; Bresser, D. The success story of graphite as a lithium-ion anode material - fundamentals, remaining challenges, and recent developments including silicon (oxide) composites. *Sustainable Energy Fuels* **2020**, *4*, 5387−5416.

(5) Xing, B.; Zeng, H.; Huang, G.; Jia, J.; Yuan, R.; Zhang, C.; Sun, Q.; Cao, Y.; Chen, Z.; Liu, B. Magnesium citrate induced growth of noodle-like porous graphitic carbons from coal tar pitch for high-performance lithium-ion batteries. *Electrochim. Acta* **2021**, *376*, 138043.

(6) Liu, S.; Loper, C. R. The Formation of Kish Graphite. *Carbon* **1991**, *29*, 547−555.

(7) Cong, J.; Cao, X.; Gao, H.; Zhao, P.; Han, Z.; La, J. An Investigation on Mechanism of Forming of Kish Graphite in the Hepereutectic Molten Iron. *J. Dalian Inst. Technol.* **1985**, *24*, 13−18.

(8) Nishimoto, H.; Daimon, H.; Suga, S.; Imada, S.; Matsushita, T.; Nakatani, T.; Namba, H.; Ohta, T.; Kagoshima, Y.; Miyahara, T. Unusual photoelectron angular distribution of Kish graphite. *J. Electron Spectrosc. Relat. Phenom.* **1996**, *78*, 465−468.

(9) Kaburagi, Y.; Hishiyama, Y. Changes in electronic properties of high quality kish graphite crystals by doping with a slight amount of iron impurities. *Carbon* **1999**, *37*, 155−158.

(10) Kaburagi, Y.; Hishiyama, Y. Electronic properties of kish graphite crystals with low values of residual resistivity ratio. *Carbon* **1998**, *36*, 1671−1676.

(11) Miura, Y.; Shimada, K.; Negishi, H.; Negishi, S.; Shiozawa, H.; Higashiguchi, M.; Tobita, N.; Chui, X. Y.; Aiura, Y.; Namatame, H.; Taniguchi, M. High-resolution angle-resolved photoemission study of kish graphite. *Phys. B Condens. Matter* **2006**, *383*, 150−151.

(12) Walker, P. L.; Imperial, G. Structure of Graphites: Graphitic Character of Kish. *Nature* **1957**, *180*, 1185.

(13) Liu, S.; Loper, C. R. Kish, a Source of Crystalline Graphite. *Carbon* **1991**, *29*, 1119−1124.

(14) Laverty, P. D.; Nicks, L. J.; Walters, L. A. *Recovery of Flake Graphite from Steelmaking Kish*; RI 9512; Bureau of Mines: United States, 1995; pp 3−23.

(15) Kazmi, K. R.; Anwar, M. S.; Bhatti, M. A.; Mehmood, A. Recovering of flake graphite from steelmaking Kish. *Pak. J. Sci. Ind. Res.* **2007**, *50*, 284−287.

(16) An, J.-C.; Kim, H. J.; Hong, I. Preparation of Kish graphite-based graphene nanoplatelets by GIC (graphite intercalation compound) via process. *J. Ind. Eng. Chem.* **2015**, *26*, 55−60.

(17) Frost, R. *The Recovery of Kish Graphite from Secondary Sources*; University of Birmingham: Birmingham, 2015.

(18) Inoue, R.; Suito, H. Flotation of Kish Graphite Precipitated from Carbon-saturated Iron Melt. *Tetsu-To-Hagane* **2009**, *76*, 538−544.

(19) Kaburagi, Y.; Asano, Y.; Hishiyama, Y. Kish graphite as a magnetic field sensor. *Carbon* **2004**, *42*, 3266−3269.

(20) Klett, J. W.; Pappano, P. J.; Boudreaux, P. J. Kish-derived graphitic heat spreaders and foils. U.S. Patent 0107551 A1, May 17, 2007.

(21) Wang, S.; Kravchyk, K. V.; Krumeich, F.; Kovalenko, M. V. Kish Graphite Flakes as a Cathode Material for an Aluminum Chloride-Graphite Battery. *ACS Appl. Mater. Interfaces* **2017**, *9*, 28478−28485.

(22) Kumari, T. S. D.; Jebaraj, A. J. J.; Raj, T. A.; Jeyakumar, D.; Kumar, T. P. A kish graphitic lithium-insertion anode material

obtained from non-biodegradable plastic waste. *Energy* **2016**, *95*, 483−493.
(23) Wang, Z.; Xing, B.; Zeng, H.; Huang, G.; Liu, X.; Guo, H.; Zhang, C.; Cao, Y.; Chen, Z. Space-confined carbonization strategy for synthesis of carbon nanosheets from glucose and coal tar pitch for high-performance lithium-ion batteries. *Appl. Surf. Sci.* **2021**, *547*, 149228.
(24) Wei, L.; Zeng, M. Separation and classification equipment for fine materials. 2013100454457A, May 15, 2013.
(25) Kang, F.; Zhang, T.-Y.; Leng, Y. Electrochemical synthesis of sulfate graphite intercalation compounds with different electrolyte concentrations. *J. Phys. Chem. Solid.* **1996**, *57*, 883−888.
(26) Loth, E. Drag of non-spherical solid particles of regular and irregular shape. *Powder Technol.* **2008**, *182*, 342−353.
(27) Tran-Cong, S.; Gay, M.; Michaelides, E. E. Drag coefficients of irregularly shaped particles. *Powder Technol.* **2004**, *139*, 21−32.
(28) Mcnown, J. S.; Malaika, J. Effects of particle shape on settling velocity at low Reynolds numbers. *Trans., Am. Geophys. Union* **1950**, *31*, 74.
(29) Bourelle, E.; Kaburagi, Y.; Hishiyama, Y.; Inagaki, M. STM study of surfaces of kish graphite doped by iron. *Carbon* **2001**, *39*, 1955−1962.
(30) Boehm, H. P.; Setton, R.; Stumpp, E. Nomenclature and terminology of graphite intercalation compounds. Report by a subgroup of the international committee for characterization and terminology of carbon and graphite on suggestions for rules for the nomenclature and terminology of graphite intercalation compounds. *Synth. Met.* **1985**, *11*, 363−371.
(31) Boehm, H. P.; Setton, R.; Stumpp, E. Nomenclature and terminology of graphite intercalation compounds. *Carbon* **1986**, *24*, 241−245.
(32) Boehm, H. P.; Setton, R.; Stumpp, E. Nomenclature and terminology of graphite intercalation compounds (IUPAC Recommendations 1994). *Pure Appl. Chem.* **1994**, *66*, 1893−1901.
(33) Noel, M.; Santhanam, R. Electrochemistry of graphite intercalation compounds. *J. Power Sources* **1998**, *72*, 53−65.
(34) Dresselhaus, M. S.; Dresselhaus, G. Intercalation compounds of graphite. *Adv. Phys.* **2002**, *51*, 1−186.
(35) Lévy, F., Intercalated Layered Materials. *Physics and Chemistry of Materials with Layered Structures*, 1 ed.; Springer Netherlands: Dordrecht, 1979; pp 1−31.
(36) Cao, N.; Shen, W.; Wen, S. The Characterization of the Porous Structures of Expanded Graphite. *Acta Phys.-Chim. Sin.* **1996**, *12*, 766−768.
(37) Lv, Y.; Xing, B.; Yi, G.; Guo, H.; Huang, G.; Zhang, C.; Liu, Q.; Zhang, X.; Cao, Y.; Li, L. Synthesis of oxygen-rich TiO2/coal-based graphene aerogel for enhanced photocatalytic activities. *Mater. Sci. Semicond. Process.* **2020**, *117*, 105169.
(38) Zheng, Y.-P.; Wang, H.-N.; Kang, F.-Y.; Wang, L.-N.; Inagaki, M. Sorption capacity of exfoliated graphite for oils-sorption in and among worm-like particles. *Carbon* **2004**, *42*, 2603−2607.
(39) Cao, N.; Shen, W.; Wen, S. Affinity Adsorption of Oil On Expanded Graphite. *Chem. Res. Appl.* **1997**, *9*, 54−56.
(40) Zhao, H.; Zhou, W.; Shen, W.; Kang, F. Pore structure of Exfoliated Graphite and Its Varieties of Liquid Sorption. *Mater. Sci. Eng.* **2002**, *20*, 153.

https://doi.org/10.1021/acsomega.1c00591
ACS Omega 2021, 6, 9868−9875